atmosphere

MDPI

Article

A 3D Monte Carlo Simulation for Aerosol Deposition onto Horizontal Surfaces by Combined Mechanisms of Brownian Diffusion and Gravity Sedimentation

Shixian Wu [1], Hui Zhu [1,*], Yongping Chen [1], Can Qi [1] and Gang Li [2]

[1] School of Energy and Building Environment, Guilin University of Aerospace Technology, Guilin 541004, China
[2] Sinosteel Maanshan General Institute of Mining Research Co., Ltd., Maanshan 243000, China
* Correspondence: zhuhui@guat.edu.cn

Abstract: A three-dimensional Monte Carlo model was developed to simulate the deposition of aerosol particles onto horizontal solid surfaces. The random walk method was employed to solve the particle transport equation, which allowed obtaining the trajectory of particle motion by a combined mechanism of Brownian diffusion and gravity sedimentation. The particle transport mechanism was described in terms of a Peclet number (*Pe*). The local structures of the dust layer, the relationship between the structure of the dust layer and particle transport mechanisms, and the number of the particles attached to the solid surface were investigated. The results showed that for a small *Pe*, when Brownian diffusion was a controlling mechanism for aerosol transport, the dust layer might exhibit a more open and looser structure, while for a large *Pe*, the dust layer was dense and tight. The differences of deposition morphologies under different transport mechanisms were caused by the different random intensities of particle motion. There was an upper limit of the maximum number of particles attached to the surface, and it strongly depended on particle transport mechanisms and size distributions. Additionally, the deposit morphologies obtained with the 3D Monte Carlo model were in good agreement with the experimental results found in the literature.

Keywords: aerosol deposition; stochastic model; horizontal surface; particle size distribution; micromorphology

Citation: Wu, S.; Zhu, H.; Chen, Y.; Qi, C.; Li, G. A 3D Monte Carlo Simulation for Aerosol Deposition onto Horizontal Surfaces by Combined Mechanisms of Brownian Diffusion and Gravity Sedimentation. *Atmosphere* **2022**, *13*, 1408. https://doi.org/10.3390/atmos13091408

Academic Editor: Jorge Pey

Received: 20 July 2022
Accepted: 30 August 2022
Published: 31 August 2022

1. Introduction

The deposition of aerosol particles onto solid surfaces is a common phenomenon in practice, such as particle deposition on indoor walls, floors and furniture surfaces, worktops in industrial ultra clean workshops, surfaces of electronic components in a cleanroom, and other similar planes [1–5]. When aerosol particles are deposited on various surfaces in indoor environments, they can cause indoor environmental pollution [6,7]. During the preparation of electronic components and semiconductor wafers, the adhesion and deposition of aerosol particles will result in many problems such as overvoltage and reduction of product yield [8]. As the size of the circuit line width decreases, particle contamination becomes more critical, especially with respect to nanoscale particles. Since particle deposition pollution is closely related to the atmospheric environment, under the background of the aggravation of haze pollution in China's urban atmospheric environment [9–11], it is vitally important to study the deposition characteristics of aerosol particles on solid surfaces.

In general, particle deposition onto solid surfaces is affected by several physical mechanisms such as gravity, thermophoresis, Brownian diffusion, and electrostatic force [12,13]. Sehmel experimentally investigated the combined effect of diffusion (eddy diffusivities and Brownian diffusion) and gravity settling over a horizontal smooth surface for particle sizes from 10^{-3} μm to 10^{2} μm; the results suggested that both Brownian and eddy diffusion contributed significantly to the diffusional mass transport [14]. Ounis et al. theoretically

analyzed the Brownian diffusion deposition of submicrometer particles from a point source in the viscous sublayer of a turbulent shear flow near a solid smooth wall [15]. It was found that the Brownian diffusion played a significant role in the diffusion deposition of submicrometer particles near the wall, and Brownian diffusivity increased as particle size decreased. Cooper et al. reported that the deposition rate rapidly increased with decreasing particle size in the range of 0.01–10 μm [16].

The effect of gravity toward the surface on particle deposition has been investigated. The most typical deposition process occurs on the surface of semiconductor wafers in a cleanroom environment. For example, Liu and Ahn carried out a theoretic calculation for the particle deposition on horizontal semiconductor wafers in the typical manufacturing environment of the cleanroom using the equations of convective diffusion and sedimentation. The results showed that the deposition velocity decreased with increasing particle size in the diffusion regime and increased with increasing particle size in the sedimentation regime, with a minimum deposition velocity occurring in the vicinity of 0.2 μm [17]. This theoretical model for particle deposition was then confirmed by their subsequent experimental investigation [18]. Yiantsios and Karabelas conducted an experimental investigation for the deposition of micron-sized glass particles on a glass substrate in a horizontal laminar flow narrow channel, and found that the effects of gravity was important for micron-sized particles [19]. Recently, Yook et al. analyzed the effects of gravitational settling as well as the Brownian diffusion of aerosol particles on deposition velocity onto a face-up wafer using the Gaussian diffusion sphere model (GDSM) [20].

In indoor environments, particle deposition onto indoor surfaces can greatly alter the indoor particle exposure level; as a result, there is an increasing interest in understanding the mechanisms controlling particle deposition. Many scholars have conducted a great deal of research on this issue. For example, Thatcher et al. reported that gravitational settling was the dominant deposition mechanism for particle diameters greater than 1 μm under natural convection flow conditions based on small-scale chamber tests [21]. Some experiments were performed in a room with different air flow conditions [22–24]. Various analytical models have been developed and applied to the estimation of the particle deposition rate on indoor surfaces [25–27], and found that the particle deposition rate was strongly dependent upon both particle size and the placement form of the deposition surface (e.g., horizontal floor or vertical wall).

However, the above studies focus on the analysis of macro parameters such as the deposition rate and deposition distribution of particles under different deposition mechanisms, and thus fail to give important information such as the micromorphological structure of solid surfaces after aerosol deposition. Experimental studies have shown that there are two typical surface depositions, i.e., monolayer deposition and multilayer deposition [28,29]. During monolayer deposition, the particles only have mechanical contact with the deposition surface, and the particles are distributed in a sparse and non-uniform state. For multilayer deposition, the particles not only contact the surface directly, but also contact with each other, resulting in the deposition morphology being completely different from the original particles. Therefore, when evaluating the risk of particle deposition pollution or taking some measures to remove the particle pollution from the contaminated surface, it is necessary to consider the deposit's micromorphology and the internal correlation between the deposition morphology and the deposition mechanism, so as to give a more accurate risk estimation and adopt a more effective particle removal scheme. In addition, in practical situations, small particles suspended in a building environment are simultaneously subjected to Brownian diffusion and gravitational forces; the relative importance of each of the mechanisms is therefore needed for a deeper understanding.

The aim of the present investigation is to analyze the process of particle deposition at a micro-level, with consideration of the combination of the Brownian diffusion and gravitational settling. The calculation model of particle deposition was established based on the diffusion-convective transport equation, and the particle trajectory was solved by using the random walk method (RWM). By tracking the spatial and temporal information of the particle movement, the

physical image of the particle deposition process was dynamically reproduced, and the physical mechanism of particle deposition morphology evolution and the microscopic characteristics of particle deposition distribution on the surface were investigated from a microscopic aspect, which provided the necessary theoretical basis for particle deposition risk estimation and effective removal technology for particle deposition pollution.

2. Mathematical Modeling

The particle deposition was considered in a box bounded by a two-dimensional deposition surface of length L, width W, and vertical extent H, as shown in Figure 1. Because of the complexity of the mechanical behaviors in a real process of particle deposition, including particle–particle, particle–surface, and particle–airflow interactions, some assumptions were made as follows: (a) The sizes of the particles were sufficiently small and were also present in a low concentration, so the particle–particle interaction was negligible. (b) The particle transport behavior took place under a calm condition, meaning that the influence of air flow on particle transport behavior could be ignored. (c) Brownian diffusion and gravity sedimentation were considered as the main mechanisms for particle deposition, so the effects of thermophoresis and electrophoresis were neglected. (d) The gravity was settled in the y direction, such that the particle had a migration velocity normal to the deposition surface. (e) The particles entering the calculation area were assumed to be spherical with the same physical parameters.

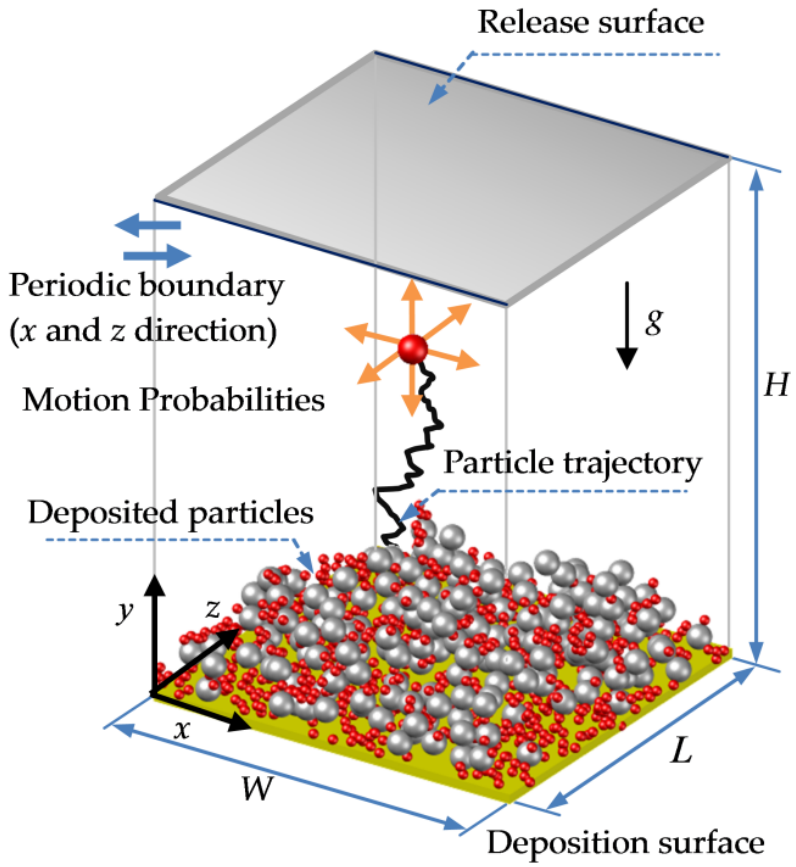

Figure 1. Model of aerosol deposition on a horizontal solid surface.

Based on the above physical assumptions, the transport equation for the particle deposition is given as [30]

$$D\frac{\partial^2 n}{\partial x^2} + D\frac{\partial^2 n}{\partial y^2} + D\frac{\partial^2 n}{\partial z^2} - u_y\frac{\partial n}{\partial y} = 0 \quad (1)$$

The first three terms in Equation (1) are the diffusion terms in the x, y, and z directions, and last term is the particle migration term in the y direction. In Equation (1), n is the number of particles per unit volume at position (x, y, z) and u_y is the migration velocity due to the gravity at position (x, y, z), known as the particle settling velocity, which can be obtained from [31]

$$u_y = \frac{\rho_p d_p^2 C_s g}{18\mu} \tag{2}$$

where ρ_p is the particle density, d_p is the particle diameter, μ is the dynamic viscosity of air, g is the gravitational acceleration, and C_s is the Cunningham slip correction, which is taken to be [32]

$$C_s = 1 + \frac{\lambda}{d_p}[2.514 + 0.8\exp(-0.55\frac{d_p}{\lambda})] \tag{3}$$

where λ is the mean free path of the surrounding fluid, which can be evaluated from the expression [33]

$$\lambda = kT/(\sqrt{2}\pi d_a^2 P) \tag{4}$$

where d_a is the diameter of air molecules and P is the fluid pressure.

The particle diffusion coefficient, D, used in Equation (1) is calculated by the equation [34]

$$D = \frac{k_B T C_s}{3\pi\mu d_p} \tag{5}$$

where k_B is the Boltzmann constant (k_B = 1.380649 × 10^{-23} J/K) and T is the absolute temperature.

In order to write Equation (1) in a dimensionless form, the dimensionless variables are introduced as follows:

$$n^* = \frac{n}{n_0},\ x^* = \frac{x}{l},\ y^* = \frac{y}{l},\ z^* = \frac{z}{l},\ Pe = \frac{u_y l}{D}$$

where n_0 is the background particle number concentration and l is the characteristic length, which is taken to be unity in the present simulations with the purpose of facilitation in the definition of Pe.

By multiplying both sides of Equation (1) by $l^2/(Dn_0)$, it may be rewritten in a dimensionless form as

$$\frac{\partial^2 n^*}{\partial x^{*2}} + \frac{\partial^2 n^*}{\partial y^{*2}} + \frac{\partial^2 n^*}{\partial z^{*2}} - Pe\frac{\partial n^*}{\partial y^*} = 0 \tag{6}$$

In the Monte Carlo simulation for particle deposition, the particle motion probabilities are derived from the macroscopic conservation equation, i.e., Equation (6). Now, letting δx^*, δy*, and δz* be the step size in the x, y, and z directions, respectively, then the discrete version of Equation (6) can be converted by the differential operators as follows:

$$\frac{\partial n^*}{\partial x^*} = (n^*_{x,y,z} - n^*_{x-1,y,z})/\delta x^* \tag{7}$$

$$\frac{\partial n^*}{\partial y^*} = (n^*_{x,y,z} - n^*_{x,y-1,z})/\delta y^* \tag{8}$$

$$\frac{\partial n^*}{\partial z^*} = (n^*_{x,y,z} - n^*_{x,y,z-1})/\delta z^* \tag{9}$$

$$\frac{\partial n^*}{\partial x^{*2}} = (n^*_{x-1,y,z} + n^*_{x+1,y,z} - 2n^*_{x,y,z})/\delta x^{*2} \tag{10}$$

$$\frac{\partial n^*}{\partial y^{*2}} = (n^*_{x,y-1,z} + n^*_{x,y+1,z} - 2n^*_{x,y,z})/\delta y^{*2} \tag{11}$$

$$\frac{\partial n^*}{\partial z^{*2}} = (n^*_{x,y,z-1} + n^*_{x,y,z+1} - 2n^*_{x,y,z})/\delta z^{*2} \tag{12}$$

By substituting Equations (7)–(9) and (10)–(12) into Equation (5), and imposing the condition of $\delta x^* = \delta y^* = \delta z^* = 1$, we obtain

$$n^*_{x,y} = \frac{n^*_{x+1,y,z}}{6+Pe} + \frac{n^*_{x-1,y,z}}{6+Pe} + \frac{n^*_{x,y+1,z}}{6+Pe} + \frac{n^*_{x,y-1,z}(1+Pe)}{6+Pe} + \frac{n^*_{x,y,z+1}}{6+Pe} + \frac{n^*_{x,y,z-1}}{6+Pe} \tag{13}$$

If we apply the relationship between particle concentration and probability of a particle moving in three-dimensional spaces to Equation (13), the probability of the particle moving in the six directions is [35,36]

$$\begin{aligned} P_{x+1,\,y,z} &= \tfrac{1}{6+Pe},\ P_{x-1,\,y,z} = \tfrac{1}{6+Pe},\ P_{x,\,y+1,z} = \tfrac{1}{6+Pe}, \\ P_{x,\,y-1,z} &= \tfrac{1+Pe}{6+Pe},\ P_{x,\,y,z+1} = \tfrac{1}{6+Pe},\ P_{x,\,y,z-1} = \tfrac{1}{6+Pe} \end{aligned} \tag{14}$$

As can be seen from Equation (14), the motion probabilities depend upon the Peclet number (i.e., *Pe*). Under the limiting condition of $Pe \to 0$, the transport probability of particles in each direction will be 1/6, and the deposition behavior is reduced to the well-known diffusion-limited deposition [37,38]. On the other hand, for the case of $Pe \to \infty$, the diffusion effect is negligible, and the gravity sedimentation is the dominant transport mechanism. In the middle region, the particle's motion is controlled by a combination of the particle diffusion and the gravity sedimentation. The *Pe* can therefore be used to describe the relative importance of these two transport mechanisms (i.e., diffusion and gravity sedimentation).

In the Monte Carlo simulations, the particles were sequentially released from the release surface $y = H$, and the x and z coordinates of the particle were chosen randomly using a uniform random number generator. Once the initial position of an approaching particle was determined, its trajectory could be obtained from the motion probability given by Equation (14). When the particle moved out of the sidewalls of the box, periodic boundary conditions were invoked. When the distance between the center of the particle and the deposition surface was less than a particle radius or when the distance between the approaching particle and any deposited particles was less than the sum of the two particles' radii, the particle was considered to be deposited. A more detailed description of the simulation procedure can be seen from the flow chart (Figure 2).

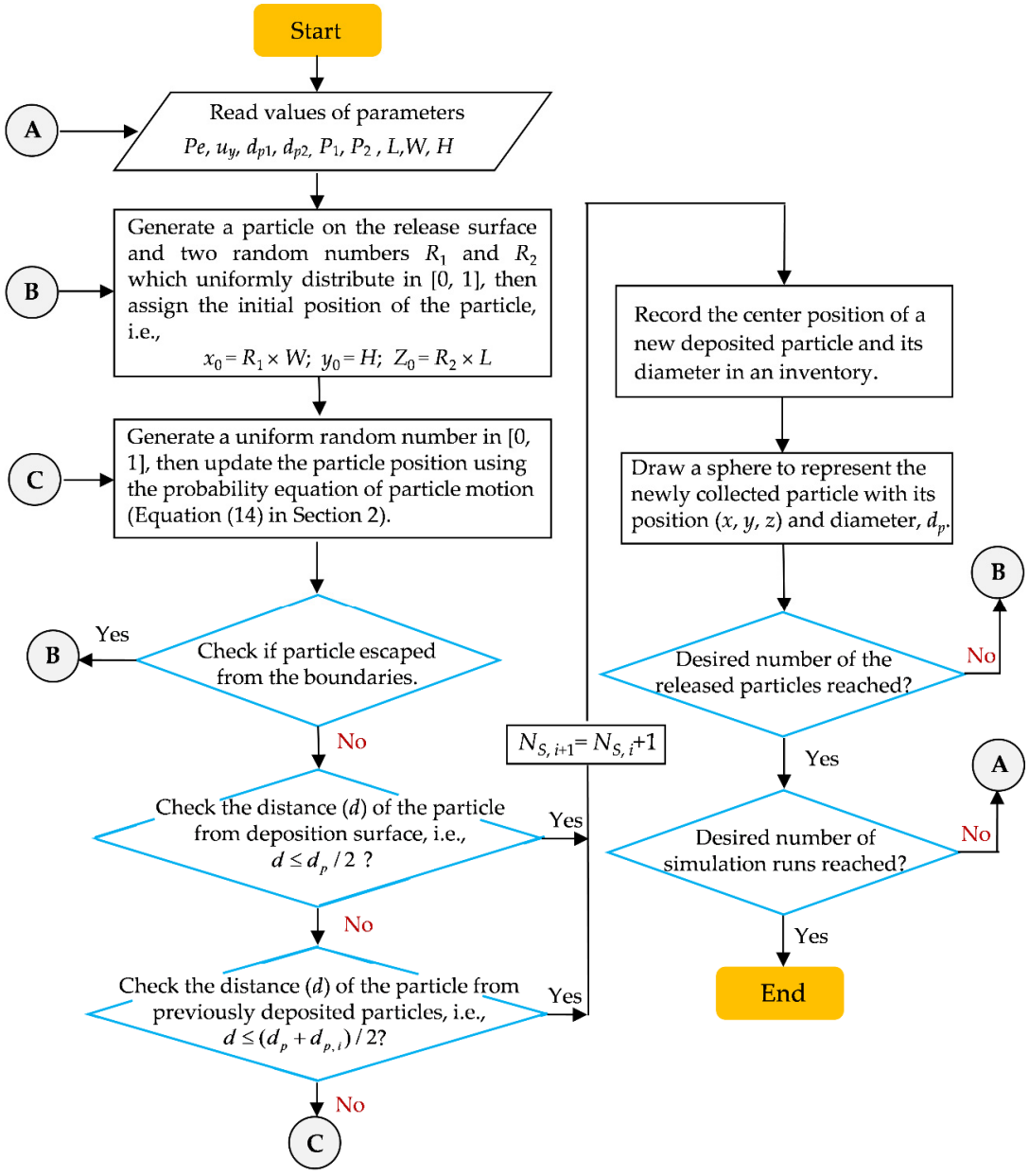

Note: N_S denotes the number of particles deposited on surface directly.

Figure 2. Schematic of the simulation algorithm for particle deposition on surface.

3. Results and Discussion

Considering the diversity of the sources of suspended particles in the actual indoor environment, the physical characteristics of the particles (particle size, particle density and size distribution, etc.) were also different [39,40], so two particle size distributions were selected as representatives to investigate the deposition behavior of polydisperse particles.

As mentioned earlier, the *Pe* represents the relative intensity of the particle's gravity sedimentation and Brownian diffusion motion. This study focused on the effects of these two motion intensities (i.e., *Pe*) on the particle deposition behavior. The physical parameters that affected the gravitational settling, such as particle density, ambient temperature, and gravitational acceleration, were included in the numerator term of the *Pe* expression, and the parameters related to the diffusion motion were included in the denominator term. For the convenience of discussion, Table 1 presents the gravitational settling velocity u_y, diffusion velocity v_d, and the corresponding *Pe*. The u_y and v_d were calculated by

Equation (2) and Equation (5), respectively, and the parameter values for the calculations of u_y and v_d were as follows: the particle density ρ_p = 2000 kg/m^3, the dynamic viscosity of air μ = 1.85 × 10^6 Pa·s, and the gravitational acceleration g = 9.8 m/s^2. The particle size distributions used in the simulations are listed in Table 2.

Table 1. Deposition velocity of aerosol particle with different sizes and Peclet numbers under standard conditions (T = 273.15 K, P = 101.325 kPa).

Particle Diameter (μm)	Diffusion Velocity (m/s)	Gravitational Sedimentation Velocity (m/s)	*Pe*
0.1	0.0024416	0.0000006	0.0002
0.2	0.0006104	0.0000024	0.0040
0.5	0.0000977	0.0000151	0.1548
1.0	0.0000244	0.0000605	2.4764
2.0	0.0000061	0.0002419	39.622
2.5	0.0000039	0.0003779	96.733
3.0	0.0000027	0.0005442	200.58
5.0	0.0000010	0.0015116	1547.7
8.0	0.0000004	0.0038697	10143
10.0	0.0000002	0.0060464	24763

Table 2. Simulation cases considered in this study.

Cases	d_{p1} (μm)	d_{p2} (μm)	P_1 (%)	P_2 (%)	L (μm)	W (μm)
Case 1	1	-	100	-	200	200
Case 2	1	2.5	80	20	200	200
Case 3	1	2.5	50	50	200	200

Note: d_{p1} and d_{p2} denote the diameters of small-sized and large-sized particles, P_1 and P_2 denote the proportion of small-sized and large-sized particles in the total particle number, and L and W denote the length and width of the deposition surface.

3.1. Validations of Computational Method

The numerical model used in this study was validated against the experimental observations given by Krinke et al. [41], and the results are shown in Figure 3. The deposition morphologies were created by the deposition of 30 nm indium particles on a silicon oxide surface. The particle number density N_p (i.e., the amount of particles per micrometer squared) on the upper image and on the lower image was 100 μm^{-2} and 420 μm^{-2}, respectively. On the right-hand side, scanning electron microscope (SEM) images of two samples are shown. On the left-hand side, the corresponding images obtained with the present computer simulation are plotted. Both the experimental and theoretical deposition morphologies showed the same characteristics. At a low particle number density, the particles were distributed mainly randomly. A few agglomerates consisting of up to four particles could be found, but most of the particles were not agglomerated. An increase of particle number density led to a formation of relatively large agglomerates and a few single particles. In this context, a single particle was a particle which was not in contact with another particle.

A quantitative comparison between the experimental results and computer simulations is shown in Figure 4. It was based on the evaluation of the amount of single particles on the deposition surface which could be easily detected on the SEM images. The ordinate in the figure represents the ratio between the amount of single particles per unit area $N_{SingleParticle}$ to the total amount of particles per unit area N_{Total}, and the abscissa is the particle number density. Two sizes of particle were used in this comparison, i.e., d_p = 30 nm (left diagram) and 50 nm (right diagram). Three independent results from the present computer simulation are presented, since the particle deposition process was characterized by randomness. It can be seen that the ratio $N_{SingleParticle}/N_{Total}$ rapidly decreased as the particle number density N_p increased, and the results obtained with the 3D Monte Carlo model were in good agreement with the experimental data. The verifications confirmed

that the proposed stochastic simulation model is capable of simulating particle deposition and then providing particle deposition morphology.

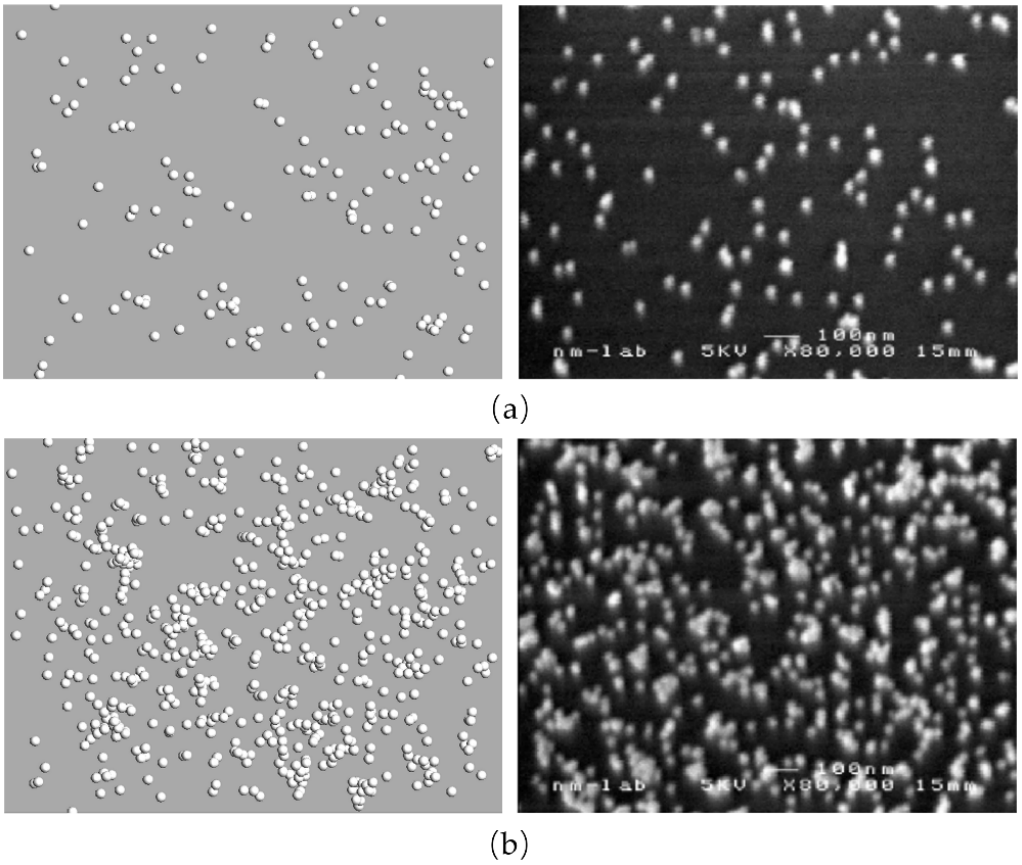

Figure 3. Comparison of experimentally determined particle deposition morphologies with the results of the computer simulations: (**a**) particle number density N_p = 100 μm^{-2} and (**b**) N_p = 420 μm^{-2}.

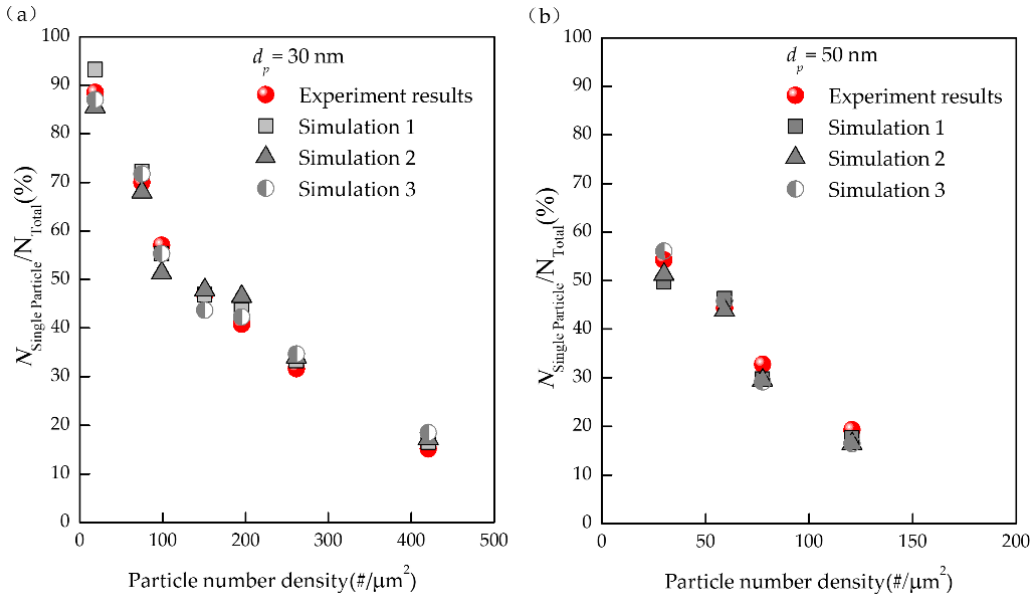

Figure 4. Comparison of particle distribution between experimental results and computer simulations: (**a**) d_p = 30 nm and (**b**) d_p = 50 nm. ("#" denotes the number of particles per unit deposition area).

3.2. Morphological Characteristics of Deposits

Figure 5 shows the morphological structure of the deposits under two particle size distributions with different *Pe*. In order to clearly show the micromorphological structure of the deposits, only the deposits on the deposition surface with an interval of 200 μm × 200 μm are presented.

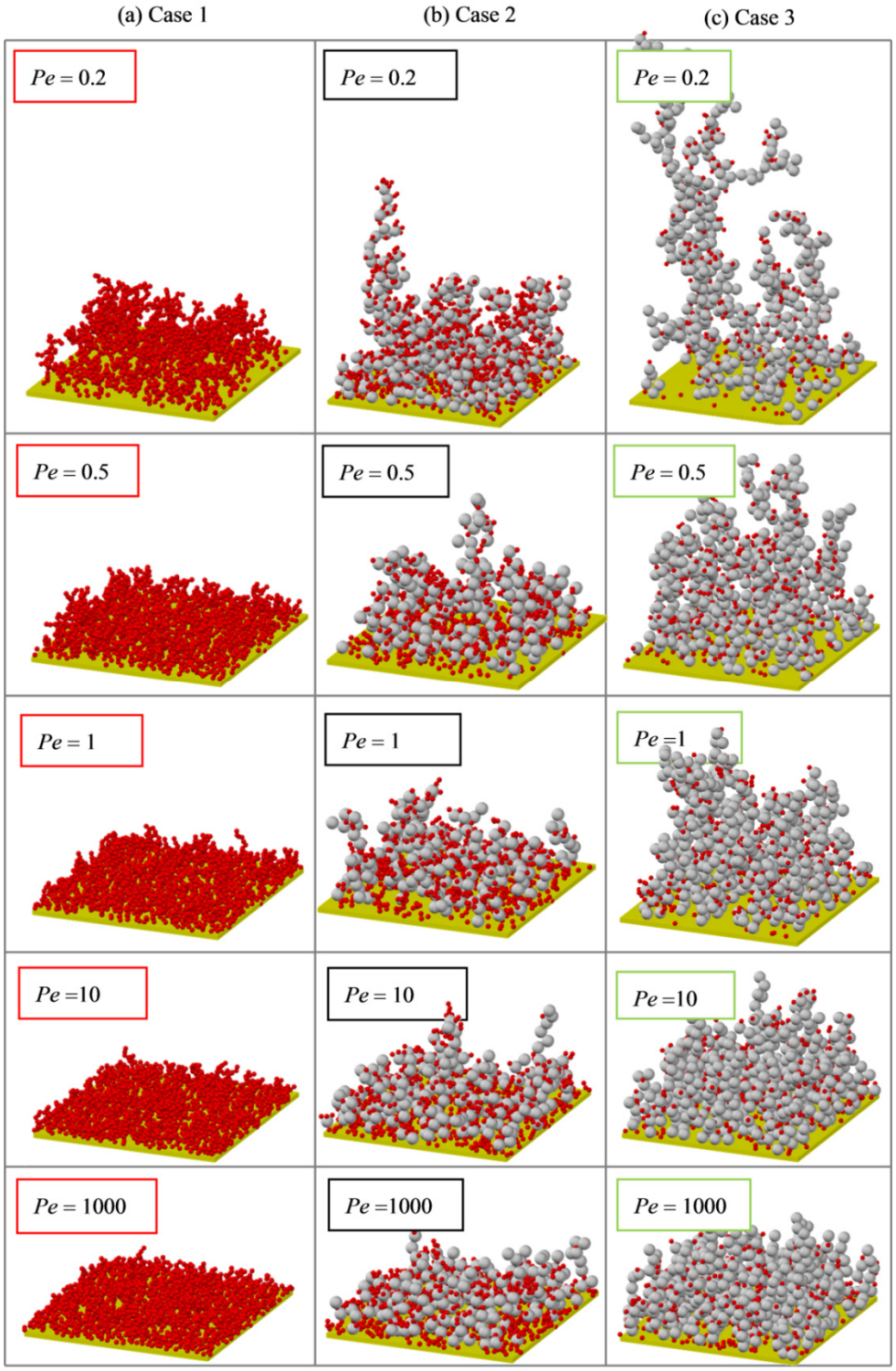

Figure 5. Deposition morphologies at different *Pe* for three kinds of particle size distributions: (**a**) Case 1; (**b**) Case 2; and (**c**) Case 3.

The particle deposition morphologies of three kinds of particle size distributions (Case 1, Case 2, and Case 3) showed the same characteristics. With the increase of *Pe*, the deposition morphologies evolved gradually from the loose floc structure to a tight packing one, and no deposit collapse caused by the existence of large particles was observed.

Figure 5 also shows that in the case of a small *Pe* ($Pe < 1$), the number of particles directly deposited on the surface was lower, and more particles were deposited on the deposited surface and formed a dust floc structure with a large spatial scale. In the case of large *Pe* ($Pe > 100$), the number of particles directly deposited on the surface increased significantly, and the accumulation of the deposits was relatively tight. Therefore, the particles in the upper layer of the deposits were more likely to be resuspended, while the particles in the sedimentary layer were less likely to be suspended due to the lower shear force of the airflow. In addition, the particle distribution on the surface showed nonuniformity under different *Pe*, and some local areas of the deposition surface had more particles deposited, while some areas had no particle deposition.

In order to explain the physical mechanism of the difference of deposit morphology and structure under different *Pe*, the particle trajectories for different *Pe* were calculated and the results are shown in Figure 6. It can be seen that when $Pe = 0.2$, the particle trajectories showed strong random walk characteristics. Due to the strong random movement of particles at small *Pe*, once particles were deposited onto the surface, the deposited particles had a greater probability of colliding with the subsequent random moving particles than in other areas that had not had particles deposited onto them. Therefore, it was very easy for the deposited particles to form a larger-scale dust floc structure; when $Pe = 100$, the particle trajectories were straight, the diffusion effect almost disappeared, and the spatial distribution of the particles was uniform, while for medium *Pe* (e.g., $Pe = 1$ and 10), the deposit morphology exhibited a transitional structure.

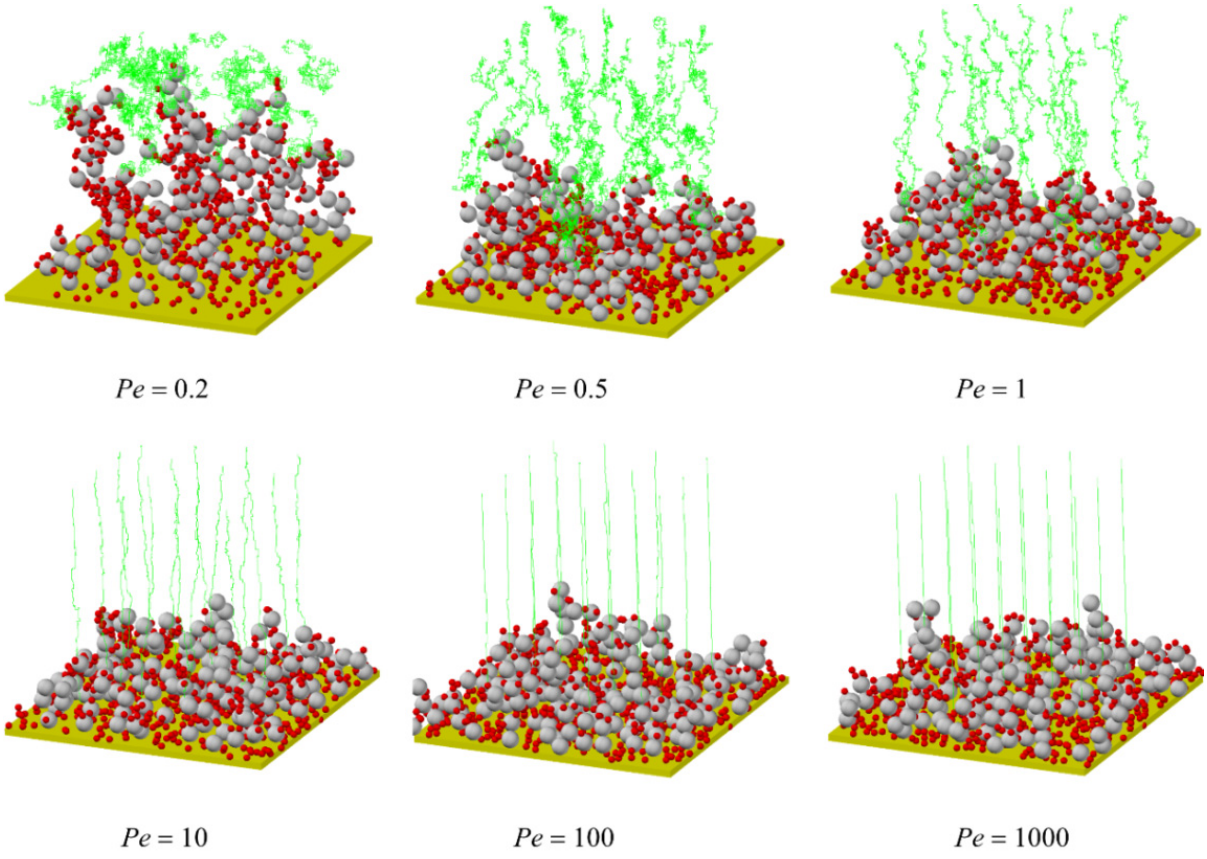

Figure 6. Trajectories of particles motion with different *Pe*.

3.3. Number of Particles Deposited on the Surface

From the morphological structure of the deposits shown in Figure 5, it could be intuitively observed that the number of particles directly deposited onto the surface was different at different *Pe*. When evaluating the possible damage and potential corrosion of the deposition surface caused by particle deposition, more attention should be paid to the number of particles that keep in contact with the surface; therefore, the relationship between the number of particles directly deposited on the surface and the particle transport mechanism as well as particle size distribution will be discussed below.

Figure 7 demonstrates the quantitative relationship between the number of particles N_S deposited directly onto the surface and the number of released particles N_G at different *Pe*, where N_S represents the particles on the deposition surface of 40 μm × 40 μm. The monodisperse particle deposition (i.e., Case 1) is shown in Figure 7a, and the polydisperse particle depositions (i.e., Case 2 and Case 3) are shown in Figure 7b,c, respectively.

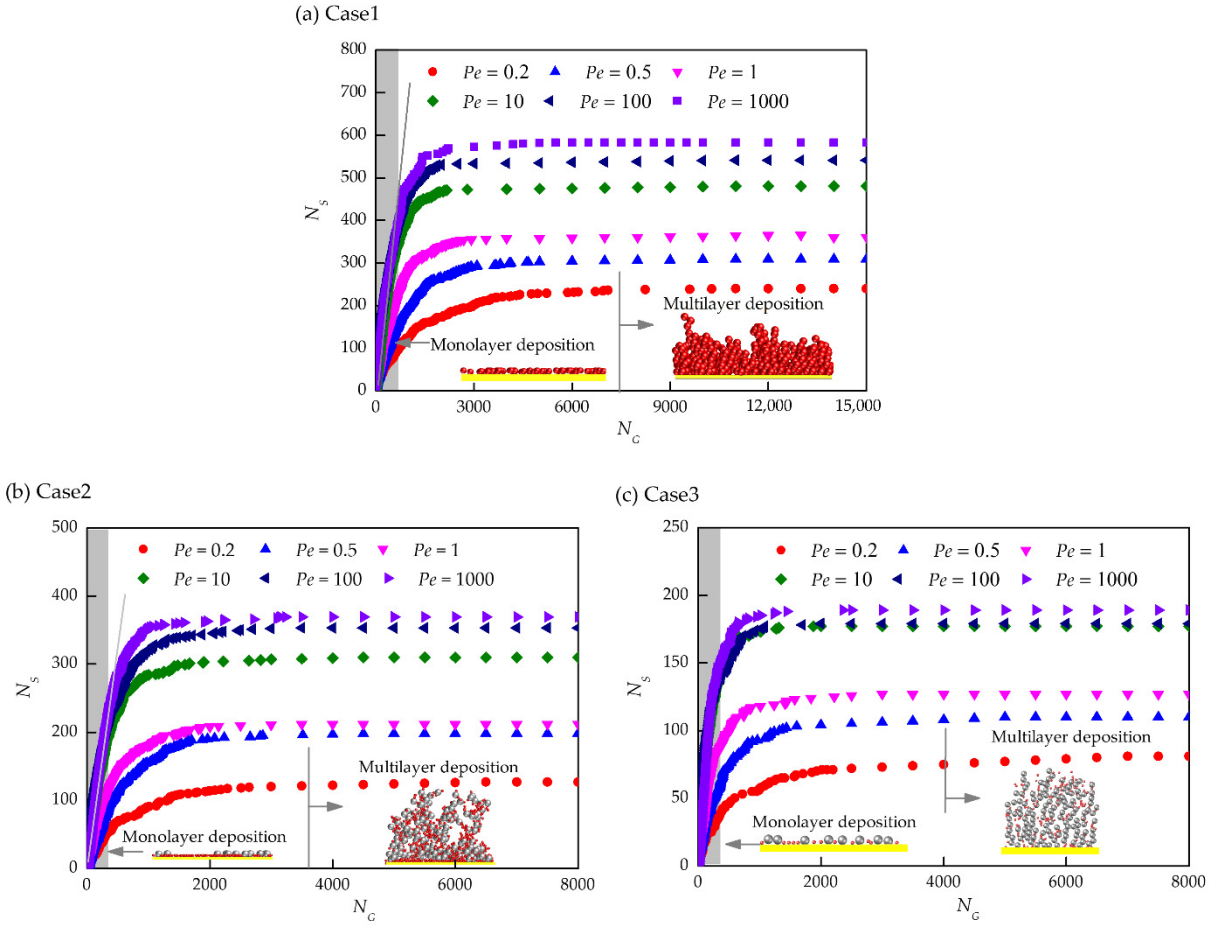

Figure 7. Relationships between the number of the particles deposited on the horizontal surface N_S and the number of the released particles N_G: (**a**) Case 1; (**b**) Case 2; and (**c**) Case 3.

For the case of monodisperse particle deposition (see Figure 7a), in the initial stage of deposition, the number of particles N_S directly deposited on the surface increased rapidly with the number of released particles N_G, and then the increased rate slowed down and finally maintained a certain value (called the maximum number of particles deposited on the surface, $N_{S,max}$), and this value increased with the increase of *Pe*. For example, when *Pe* = 0.2, $N_{S,max}$ = 240, and when *Pe* increased to 1000, then $N_{S,max}$ = 572; these simulation results are consistent with the observed results of the deposit morphological structure shown in Figure 8a.

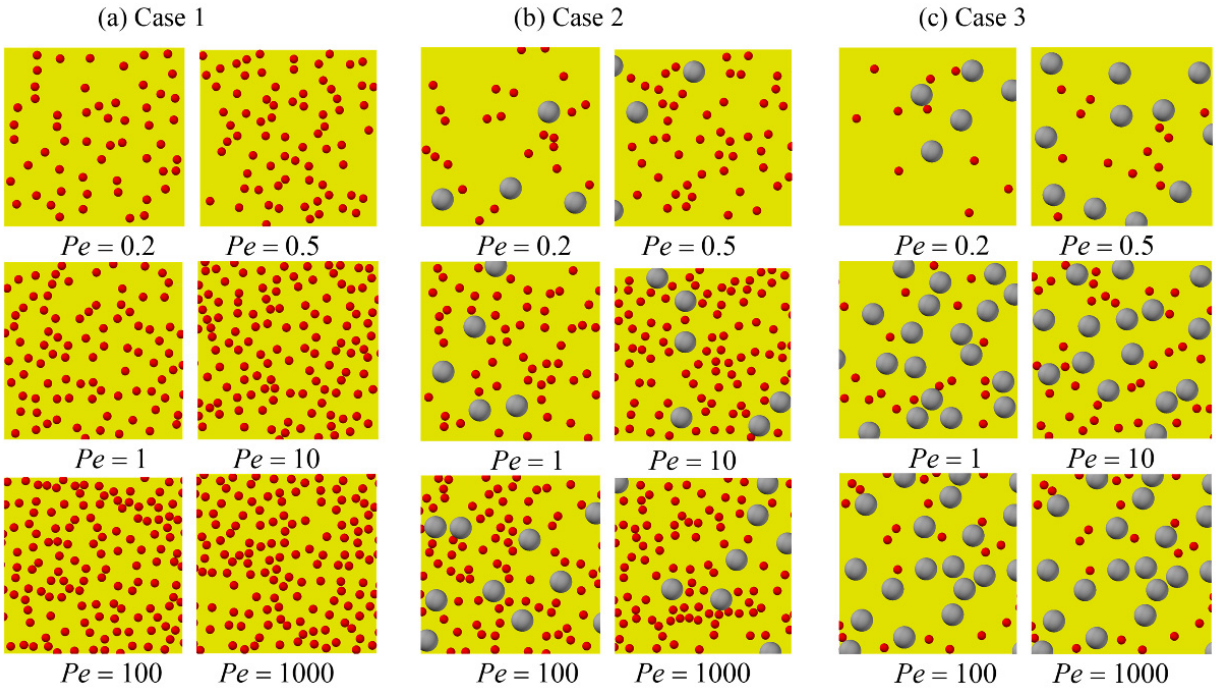

Figure 8. Deposition distributions of particles on deposition surface under different *Pe* for three kinds of particle size distributions: (**a**) Case 1; (**b**) Case 2; and (**c**) Case 3.

The abovementioned relationship between N_S and N_G also reflected that, in the initial stage of deposition, all the approaching particles could be directly deposited onto the surface, and there was no mutual accumulation of particles. This stage was therefore called monolayer deposition (gray area in Figure 7). In the monolayer deposition stage, the relationship between N_S versus N_G was approximately linear and hardly affected by *Pe*; with the increase of the number of particles deposited on the surface, the mutual accumulation between particles became more significant, and more particles tended to be deposited on the already deposited particles, so the deposition behavior gradually evolved to multilayer deposition. In the later stage of the deposition process, N_S no longer increased with the increase of N_G, which indicated that all the particles involved in the deposition events were deposited onto the previously deposited particles. The deposition surface was no longer in contact with new particles, and this stage was called the multilayer deposition stage. The intermediate stage between these two stages could be regarded as a transition stage.

The results in Figure 7 also show that in the case of polydisperse particles, the transport mechanisms (i.e., *Pe*) still played a dominant role in the particle deposition behavior. Comparing the results of Figure 7a,b, it can be seen that after adding 20% large particles (d_p = 2.5 μm) in the original single particle size distribution (d_p = 1 μm), the curve of N_S versus N_G in the case of *Pe* = 1 was very close to the results of *Pe* = 0.5, meaning that the number of particles deposited onto the surface directly was almost the same for these two *Pe*, as shown in Figure 8b. However, when the proportion of large particles in the particle group reached 50%, no results similar to those in Figure 7c were observed. On the contrary, the increase of the number of large particles made the deposition behavior shift towards the large *Pe*. For example, the relationship for N_S versus N_G at *Pe* = 1 was close to the result at *Pe* = 100. This phenomenon can be observed from the deposition morphologies in Figure 8c.

It can be seen from the above simulation results that no matter what the conditions of particle deposition were, the number of particles directly deposited onto the surface had an upper limit (i.e., the maximum number of particles deposited on the surface, $N_{S,max}$), and this upper limit was related to both the transport mechanism and particle size distribution.

In order to clearly describe the relationship between $N_{S,max}$ and the transport mechanism (i.e., *Pe*), $N_{S,max}$ was plotted as a function of *Pe* for three kinds of particle size distributions, as shown in Figure 9. The results show that in the range of $0.2 \leq Pe \leq 100$ (gray area in the Figure 9), $N_{S,max}$ was sensitive to *Pe* for the three particle size distributions, i.e., $N_{S,max}$ increased with the increase of *Pe*, while in the range of $Pe < 0.2$ to $Pe > 100$, $N_{S,max}$ had almost nothing to do with *Pe*.

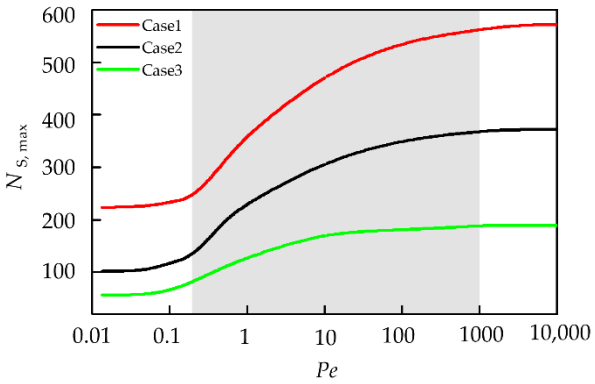

Figure 9. Relationships between maximum number of particles attached to the surface $N_{S,max}$ and *Pe* for three kinds of particle size distributions.

4. Conclusions

The deposition of aerosol particles onto horizontal solid surfaces by the combined mechanisms of Brownian diffusion and gravity sedimentation was studied by using three-dimensional Monte Carlo simulation techniques. Based on the results and discussion, some conclusions are summarized as follows:

(1) The particle transport mechanism was the determinant factor that affected the morphological evolution of particle deposits on the solid surface. With the increase of *Pe*, the deposits gradually evolved from a loose dust floc structure to a relatively compact packing structure, while the effect of particle size distribution on the deposit morphology only played a role in a certain range of *Pe*.

(2) The characteristics of particle trajectories under different transport mechanisms were the physical essence of the evolution of the deposit morphology. In the case of a small *Pe* ($Pe < 1$), the particle trajectories exhibited a strong random walk characteristic; when $Pe > 100$, the particles almost moved in a straight line; and for a medium *Pe* ($1 < Pe < 100$), the randomness of the particle trajectories was between these two cases.

(3) According to the time series of the particle deposition process, it could be divided into monolayer deposition, transitional deposition, and multilayer deposition. In the monolayer deposition stage, the particles were completely deposited on the surface, while in the multilayer deposition stage, all particles were deposited onto the previously deposited particles, and the deposition surface no longer captured new particles regardless of the deposition conditions.

(4) There was an upper limit for the number of particles directly deposited onto the surface (i.e., the maximum number of particles deposited on the surface), and this upper limit was related to the particle transport mechanism and particle size distribution.

Author Contributions: Conceptualization, S.W. and H.Z.; methodology, H.Z.; software, H.Z. and C.Q.; validation, S.W., H.Z. and Y.C.; formal analysis, S.W.; investigation, Y.C.; resources, G.L.; data curation, S.W.; writing—original draft preparation, S.W; writing—review and editing, S.W., H.Z. and Y.C.; visualization, H.Z., G.L. and C.Q.; supervision, H.Z.; project administration, H.Z.; funding acquisition, S.W. and H.Z. All authors have read and agreed to the published version of the manuscript.

Funding: This research was funded by the National Natural Science Foundation of China (grant number 51864014), Natural Science Foundation of Guangxi Zhuang Autonomous Region (grant number 2021GXNSFAA220079), Natural Science Foundation of Guilin University of Aerospace Technology (grant number XJ20KT13), and Key Science and Technology Projects in Transportation Industry of Ministry of Transport, China (grant number 2021-MS5-126).

Institutional Review Board Statement: Not applicable.

Informed Consent Statement: Not applicable.

Data Availability Statement: Not applicable.

Acknowledgments: We would like to thank the editors and reviewers for their key work.

Conflicts of Interest: The authors declare no conflict of interest. The funders had no role in the design of the study; in the collection, analyses, or interpretation of data; in the writing of the manuscript; or in the decision to publish the results.

References

1. Lai, A.C.K. Modeling indoor coarse particle deposition onto smooth and rough vertical surfaces. *Atmos. Environ.* **2005**, *39*, 3823–3830.
2. Sipploa, M.R.; Nazaroff, W.W. Modeling particle deposition in ventilation ducts. *Atmos. Environ.* **2003**, *37*, 5597–5609.
3. Tsai, R.; Chang, Y.P.; Lin, T.Y. Combined effects of thermophoresis and electrophoresis on particle deposition onto a wafer. *J. Aerosol Sci.* **1998**, *20*, 811–825.
4. Wan, Y.; Yan, C.W.; Qu, Q. Atmospheric corrosion behavior of A3 steel by ammonium sulfate particle deposition. *Acta Phys.-Chim. Sin.* **2002**, *18*, 156–160.
5. Zhou, C.L. Pollution control engineering in the whole process of spacecraft development. *Spacecr. Environ. Eng.* **2005**, *22*, 335–341.
6. Nazaroff, W.W. Indoor particle dynamics. *Indoor Air* **2004**, *14*, 175–183. [PubMed]
7. Ali, M.U.; Lin, S.; Yousaf, B. Pollution characteristics, mechanism of toxicity and health effects of the ultrafine particles in the indoor environment: Current status and future perspectives. *Crit. Rev. Environ. Sci. Technol.* **2022**, *52*, 436–473.
8. Reinhardt, K.A.; Kern, W. *Handbook of Silicon Wafer Cleaning Technology*, 3rd ed.; William Andrew: Oxford, UK, 2018; pp. 109–126.
9. Sun, Y.; Ma, Z.F.; Niu, T. Climate change characteristics of fog days and haze days in China in the last 40 years. *Clim. Environ. Res.* **2013**, *18*, 397–406.
10. Ding, Y.H.; Liu, Y.J. Long-term variation characteristics of fog and haze in my country in the past 50 years and their relationship with atmospheric humidity. *Sci. China Earth Sci.* **2014**, *44*, 37–48.
11. Liu, X.H.; Zhu, B.; Wang, H.L. Distribution characteristics and influencing factors of haze in the Yangtze River Delta region from 1980 to 2009. *China Environ. Sci.* **2013**, *11*, 1929–1936.
12. Peters, M.H.; Cooper, D.W.; Miller, R.J. The effects of electrostatic and inertial forces on the diffusive deposition of small particles onto large disks: Viscous axisymmetric stagnation point flow approximations. *J. Aerosol Sci.* **1989**, *20*, 123–136.
13. Woo, S.H.; Lee, S.C.; Yook, S.J. Statistical Lagrangian particle tracking approach to investigate the effect of thermophoresis on particle deposition onto a face-up flat surface in a parallel airflow. *J. Aerosol Sci.* **2012**, *44*, 1–10.
14. Sehmel, G.A. Particle diffusivities and deposition velocities over a horizontal smooth surface. *J. Colloid Interface Sci.* **1971**, *37*, 891–906.
15. Ounis, H.; Ahmadi, G.; McLaughlin, J.B. Brownian diffusion of submicrometer particles in the viscous sublayer. *J. Colloid Interface Sci.* **1991**, *143*, 266–277.
16. Cooper, D.W.; Miller, R.J.; WU, J.J. Deposition of submicron aerosol particles during integrated circuit manufacturing: Theory. *Part. Sci. Technol.* **1990**, *8*, 209–224.
17. Liu, B.Y.H.; Ahn, K. Particle deposition on semiconductor wafers. *Aerosol Sci. Technol.* **1987**, *6*, 215–224.
18. Pui, D.Y.H.; Ye, Y.; Liu, B.Y.H. Experimental study of particle deposition on semiconductor wafers. *Aerosol Sci. Technol.* **1990**, *12*, 795–804.
19. Yiantsios, S.G.; Karabelas, A.J. The effect of gravity on the deposition of micron-sized particles on smooth surfaces. *Int. J. Multiph. Flow* **1998**, *24*, 283–293.
20. Yook, S.J.; Asbach, C.; Ahn, K.H. Particle deposition velocity onto a face-up flat surface in a laminar parallel flow considering Brownian diffusion and gravitational settling. *J. Aerosol Sci.* **2010**, *41*, 911–920.
21. Thatcher, T.L.; Fairchild, W.A.; Nazaroff, W.W. Particle deposition from natural convection enclosure flow onto smooth surfaces. *Aerosol Sci. Technol.* **1996**, *25*, 359–374.
22. He, C.; Morawska, L.; Gilbert, D. Particle deposition rates in residential houses. *Atmos. Environ.* **2005**, *39*, 3891–3899.
23. Thatcher, T.L.; Lai, A.C.K.; Moreno-Jackson, R. Effects of room furnishings and air speed on particle deposition rates indoors. *Atmos. Environ.* **2002**, *36*, 1811–1819.
24. Costa, D.; Malet, J.; Gehin, E. Dry aerosol particle deposition on indoor surfaces: Review of direct measurement techniques. *Aerosol Sci. Technol.* **2022**, *56*, 261–280.

25. Zhao, B.; Wu, J. Particle deposition in indoor environments: Analysis of influencing factors. *J. Hazard. Mater.* **2007**, *147*, 439–448. [PubMed]
26. Gao, N.P.; Niu, J.L. Modeling particle dispersion and deposition in indoor environments. *Atmos. Environ.* **2007**, *41*, 3862–3876.
27. Zhang, Z.; Chen, Q. Prediction of particle deposition onto indoor surfaces by CFD with a modified Lagrangian method. *Atmos. Environ.* **2009**, *43*, 319–328.
28. Lazaridis, M.; Drossinos, Y. Multilayer resuspension of small identical particles by turbulent flow. *Aerosol. Sci. Technol.* **1998**, *28*, 548–560.
29. Barth, T.; Reiche, M.; Banowski, M. Experimental investigation of multilayer particle deposition and resuspension between periodic steps in turbulent flows. *J. Aerosol. Sci.* **2013**, *64*, 111–124.
30. Friendlander, S.K. *Smoke, Dust and Haze: Fundamentals of Aerosol Dynamics*, 2nd ed.; Oxford University Press: New York, NY, USA, 2000; pp. 27–30.
31. Cheng, N.S. Comparison of formulas for drag coefficient and settling velocity of spherical particles. *Powder Technol.* **2009**, *189*, 395–398.
32. Li, A.; Ahmadi, G. Dispersion and deposition of spherical particles from point sources in a turbulent channel flow. *Aerosol Sci. Technol.* **1992**, *16*, 209–226.
33. Yates, J.T.; Johnson, J.K. *Molecular Physical Chemistry for Engineers*; University Science Books Press: Sausalito, CA, USA, 2007; pp. 317–320.
34. Hinds, W.C. *Aerosol Technology: Properties, Behavior, and Measurement of Airborne Particles*, 2nd ed.; John Wiley & Sons, Inc.: Hoboken, NJ, USA, 1999; pp. 152–153.
35. Huang, W.G.; Hibbert, D. Fast fractal growth with diffusion, convection and migration by computer simulation: Effects of voltage on probability, morphology and fractal dimension of electrochemical growth in a rectangular cell. *Phys. A* **1996**, *233*, 888–896.
36. Huang, W.G.; Hibbert, D. Computer modeling of electrochemical growth with convection and migration in a rectangular cell. *Phys. Rev. E* **1996**, *53*, 727–730. [CrossRef]
37. Witten, T.A.; Sander, L.M. Diffusion-limited aggregation. *Phys. Rev. B* **1983**, *27*, 5686–5697. [CrossRef]
38. Meakin, P. Effects of particle drift on diffusion-limited aggregation. *Phys. Rev. B* **1983**, *28*, 5221–5224. [CrossRef]
39. Zhao, H.Y.; Shao, L.Y.; Wang, Y.B. Microscopic morphology and particle size distribution of indoor air PM10 in Beijing in winter. *China Environ. Sci.* **2004**, *24*, 505–508.
40. Lang, F.L.; Yan, W.Q.; Zhang, Q. Characteristics of particle size distribution and its correlation with meteorological conditions in atmospheric particulate matter in Beijing. *China Environ. Sci.* **2013**, *33*, 1153–1159.
41. Krinke, T.J.; Deppert, K.; Magnusson, M.H. Microscopic aspects of the deposition of nanoparticles from the gas phase. *J. Aerosol Sci.* **2002**, *33*, 1341–1359.